BIOCHEMISTRY
including biophysical chemistry & molecular biology

Article

pubs.acs.org/biochemistry

Unraveling the Molecular Structure of the Catalytic Domain of Matrix Metalloproteinase-2 in Complex with a Triple-Helical Peptide by Means of Molecular Dynamics Simulations

Natalia Díaz,* Dimas Suárez, and Haydeé Valdés

Departamento de Química Física y Analítica, Universidad de Oviedo, Julián Clavería 8, Oviedo (Asturias) 33006, Spain

Supporting Information

ABSTRACT: Herein, we present the results of a computational study that employed various simulation methodologies to build and validate a series of molecular models of a synthetic triple-helical peptide (fTHP-5) both in its native state and in a prereactive complex with the catalytic domain of the MMP-2 enzyme. First, the structure and dynamical properties of the fTHP-5 substrate are investigated by means of molecular dynamics (MD) simulations. Then, the propensity of each of the three peptide chains in fTHP-5 to be distorted around the scissile peptide bond is assessed by carrying out potential of mean force calculations. Subsequently, the distorted geometries of fTHP-5 are docked within the MMP-2 active site following a semirigid protocol, and the most stable docked structures are fully relaxed and characterized by extensive MD simulations in explicit solvent. Following a similar approach, we also investigate a hypothetical ternary complex formed between two MMP-2 catalytic units and a single fTHP-5 molecule. Overall, our models for the MMP-2/fTHP-5 complexes unveil the extent to which the triple helix is distorted to allow the accommodation of an individual peptide chain within the MMP active site.

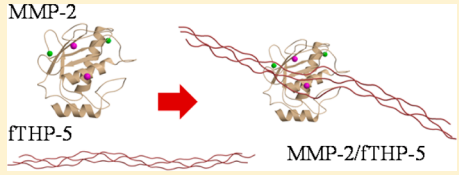

Matrix metalloproteinases (MMPs) constitute a family of zinc- and calcium-dependent enzymes involved in the hydrolysis of a variety of proteins in the extracellular environment.[1] Proteomics efforts have characterized different MMP substrates, allowing the assignment of functional roles to these enzymes during matrix remodeling, growth factor and cytokine release, and inflammation and immune responses.[2,3] As a result, MMPs are considered to be principal mediators of important physiological processes like morphogenesis, wound healing, and tissue repair, but their hydrolytic activity has been also linked to the progression of arthritis, cancer, and cardiovascular diseases.[4,5]

In animals, the extracellular matrix is an intricate network of macromolecules that, in addition to providing mechanical properties to tissues, also contributes to modulate cellular activity.[6,7] Collagen is the most abundant protein in the extracellular environment where the MMPs operate. Its prevailing tridimensional structure is a triple helix, which makes collagen highly resistant toward most proteinases, except several members of the MMP family.[8] However, structural analyses have shown that the triple helix of collagen is too wide to be accommodated within the active site of the MMPs, raising numerous questions concerning how collagen degradation proceeds.[9,10]

The original models for the collagen triple-helix structure were based on low-resolution fiber diffraction data.[11,12] In addition, high-resolution structures of a limited number of triple-helical peptides (THPs) have provided new insight into the hydration, hydrogen bonding, and sequence-dependent helical parameters in collagen.[13−19] All of the crystal structures of THPs are slight variants of the most abundant collagen sequence that consists on the repetition of several Gly−Pro−Hyp triplets per chain (Hyp stands for 4*R*-hydroxyproline). Only two examples of THP structures include a small fragment of a real collagen sequence,[14,20] so the molecular details of most of the THPs synthetized to date as models of biologically relevant collagen fragments remains unsolved.

THP molecules were initially designed to establish relationships between amino acid sequence and triple-helix stability.[21] In addition, a few THPs have been tested as collagenous biomaterials with a promising future in wound-healing applications.[12] The interaction of collagen with other macromolecules has also been analyzed using these small collagen models.[22] Thus, kinetic parameters for MMP binding to and/or hydrolyzing a variety of THPs have been reported in several studies.[23−28] Interestingly, the MMPs hydrolyze analogous peptide bonds in natural collagen and in the corresponding THP models. In addition, it has been shown that the isolated catalytic domain of the MMPs possesses triple-helical peptidase activity against THPs but not against collagen.[26,29] The reported K_m values are larger for the THPs than for the corresponding natural collagens, suggesting that the longer collagen molecule establishes additional interactions with the enzyme compared to those present in the MMP···THP complexes. However, detailed structural data for a THP or collagen molecule interacting to or bound within an MMP active site are still scarce.

Initial modeling of MMP interactions with triple-helical substrates confirmed that the active-site cleft in the catalytic

Received: August 20, 2013
Revised: October 22, 2013
Published: October 28, 2013

   dx.doi.org/10.1021/bi401144p | *Biochemistry* 2013, 52, 8556−8569

Scheme 1

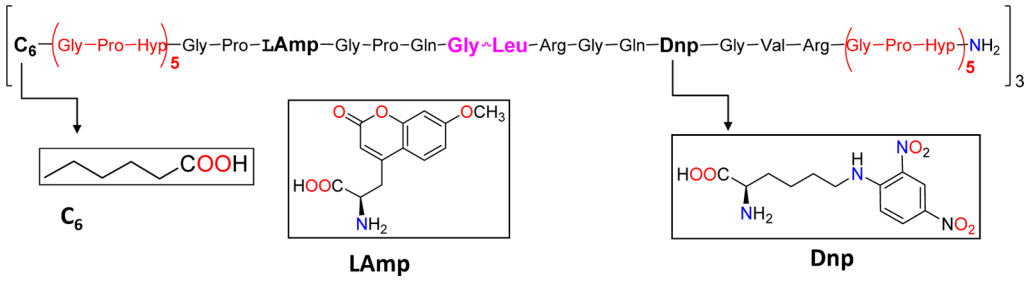

domain of the MMPs is not able to accommodate an intact triple helix.[29−31] A single α chain has to be slightly freed from the triple-helical association and aligned, under considerable rearrangement of the scissile peptide bond backbone, within the active-site cleft by forming β-strand-like hydrogen bonds.[28] Thus, the MMPs must locally unwind triple-helical collagen before they hydrolyze the peptide bonds.[9] Atomic force microscopy has allowed the direct visualization of MMP-9 during its interaction with collagen II fragments.[10] In addition, protein−protein docking analyses complemented with NMR measurements have been employed to gain some insight on the interaction of a mutant MMP-1 enzyme with a THP model of collagen I.[32] Finally, the Glu200Ala mutant form of the MMP-1 enzyme has been observed by X-ray crystallography in a nonproductive complex (the scissile peptide bond is not placed within the active site) with a THP model of collagen II.[33]

On the basis of different computational techniques and molecular models generated in previous work, the main aim of this article is to build a realistic molecular model of the prereactive complex formed between a synthetic THP molecule and the catalytic domain of an MMP in its active form. To this end, we selected a fluorogenic triple helix called fTHP-5 and the catalytic domain of the MMP-2 enzyme. On one hand, MMP-2 is the most ubiquitous matrix metalloproteinase in vertebrates, where it degrades different types of collagen, fibronectin, elastin, and all types of unfolded collagens.[34] In addition, it has been identified as a validated target for cancer therapy.[35] On the other hand, fTHP-5 is a model for the α1 chain of collagen type II in the region that is specifically recognized by the MMPs (Scheme 1).[23] The design of the fTHP-5 model introduced several modifications in the α1(II) sequence to place a fluorophore at P_5 and a quencher at P_5'. In addition, five Gly−Pro−Hyp triplets were added at each end to improve the global stability of the helix (T_m = 41 °C). Kinetic analyses confirmed that this triple helix is recognized by MMP-2 (K_m = 2.0 μM and k_{cat} = 0.049 s^{-1}) and that the enzyme cleaved fTHP-5 at the Gly(P_1)−Leu(P_1') and Gly(P_3')−Gln(P_4') peptide bonds (Gly_{775}−Leu_{776} and Gly_{778}−Gln_{779} in the collagen II triple helix).[23]

Our computational work started by building an initial structure for the fTHP-5 molecule, and taking into account previous parametrization results,[36] we investigated the dynamical behavior of the THP by means of molecular dynamics (MD) simulations. Once the stable structure of the fTHP-5 molecule is known, we investigated the intrinsic propensity of each of the three α chains in the fTHP-5 molecule to bind the MMP-2 active site. Thus, we performed potential of mean force (PMF) calculations to estimate the energy profile for the partial unwinding of each THP chain around the scissile peptide bond, evolving from a helical conformation to a nearly β-strand conformation that can enter the MMP-2 binding crevice. From the PMF simulations, the distorted geometries of the fTHP-5 molecules were then docked within the MMP-2 active site following a semirigid protocol and using molecular-mechanics Poisson−Boltzmann (MM−PB) scoring. The most stable docked structures were fully relaxed and characterized by extensive MD simulations in explicit solvent. As a result, we obtained models for fTHP-5 binding within the MMP-2 active site that unveil the extent to which the triple helix is distorted to allow the accommodation of an individual α chain within the MMP active site as well as the contacts that could drive this deformation. Following a similar approach, we also built a computational model of a hypothetical ternary complex formed between two MMP-2 catalytic units and a single fTHP-5 molecule. Overall, the various MMP-2/fTHP5 models provide new insight into the catalytic mode of action of MMP-2 and constitute a firm basis for future studies on the role played by the rest of the characteristic MMP domains in the recognition and/or destabilization of either THP or natural collagen.

MATERIALS AND METHODS

Scheme 2 outlines the workflow of the methodologies and procedures that were used to construct the most likely MMP-2/fTHP-5 models and that will be described in detail.

Scheme 2

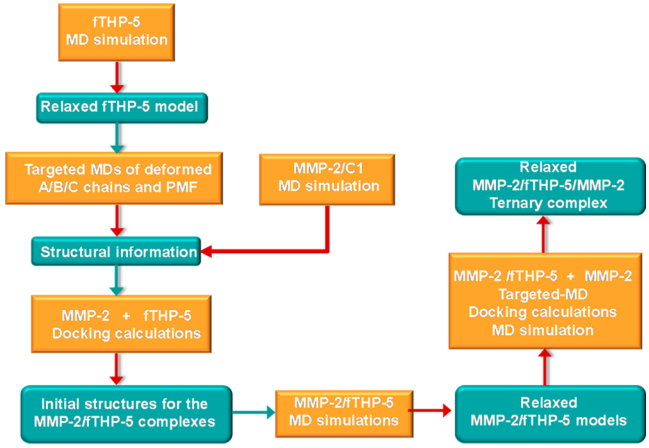

MD Simulation of the fTHP-5 Molecule in Aqueous Solution. Initial coordinates for the fTHP-5 backbone atoms were built from the amino acids sequence using the TCL/TK triple-helical collagen building script (THe BuScr).[37] This program, which is based on a statistical parametrization of the triple helix derived from the available X-ray structures of short THPs,[38] readily works with standard residues (including hydroxyproline) but requires additional data (helical propensities) for nonstandard residues. For this reason, the nonstandard

dx.doi.org/10.1021/bi401144p | Biochemistry 2013, 52, 8556−8569

residues L-2-amino-3-(7-methoxy-4-coumaryl) propionic acid (L-Amp) and *N*-2,4-dinitrophenyl (Dnp) were initially replaced by the standard amino acids serine and lysine, respectively, in the primary sequence included in THe BuScr. Subsequently, we edited the file with the coordinates of the backbone atoms in the initial triple-helical structure to obtain the fTHP-5 sequence shown in Scheme 1 and to include the N-terminal hexanoic acid (C_6). Finally, the side chains for the standard and nonstandard residues were added using the LeAP program of Amber 9.[39]

The nonstandard L-Amp, Dnp, Hyp, and C_6 residues were parametrized within the context of the parm03 AMBER force field.[40] Thus, these residues capped with Ace and Nme groups were optimized in solution (ether) at the HF/6-31G** level of theory exploring several conformers (four for L-Amp and three for Dnp). Then, the electrostatic potential, computed at the B3LYP/cc-pVTZ level of theory[41,42] using the IEF-PCM model,[43] was employed in a two-step RESP procedure[44] to obtain the atomic charges. Some missing parameters in the parm03 force field for the NO_2 substituent in Dnp were taken from the parm99 and the gaff force fields.[45,46]

The geometry of the nonstandard residues was initially relaxed within the triple helix by restrained minimizations and molecular dynamics (MD) simulations using the SANDER module of Amber10.[47] Thus, all residues but the nonstandard ones were harmonically restrained using a force constant of 100 kcal/(mol Å^2) during the following calculations that employed a generalized Born (GB) continuum solvent model for water:[48] (a) 2500 cycles of energy minimization; (b) three consecutive MD simulations (100 ps each) at 400, 350, and 300 K; and (c) 2500 cycles of energy minimization. Subsequently, fTHP-5 was surrounded by a water box that extended 25 Å from the protein atoms, which resulted in an approximate box size of 76 × 82 × 199 Å^3 (~35 000 water molecules). Six Cl^- counterions were included to neutralize the system.

Solvent molecules and counterions were conveniently relaxed by running energy minimizations and a 50 ps long MD simulation. Prior to thermalization, fTHP-5 was minimized so that the removal of bad contacts in the initial geometries is guaranteed. The solvated fTHP-5 was gradually heated to 300 K during 120 ps of MD. Then, Langevin dynamics was employed to control the temperature (300 K) using a damping factor of 2 ps^{-1}. Periodic boundary conditions were applied, and the PME approach was used for nonbonded interactions.[49] The time step of integration was 2.0 fs, and the SHAKE procedure was applied to every X−H bond.[50] A 50 ns MD simulation was run using the NAMD program.[51] Coordinates were saved every 2000 time steps, and analyses were performed for the last 40 ns.

Targeted MD Simulations and Potential Mean Force Calculations on the fTHP-5 System. We carried out a series of three targeted MD simulations and PMF calculations to force the central region of one of the A, B, or C chains of fTHP-5 to adopt a conformation that could be more prone to binding by MMP-2. The initial THP coordinates for the relaxed fTHP-5 (A state) were taken from the model generated by THe BuScr and refined with LEaP. Subsequently, this model was immersed in a water box that extended 15 Å from the solute atoms (we employed a smaller solvent box in the expensive PMF calculations than the one used in the previous MD simulations to save computer time). The system was then subjected to energy minimization and thermalization using the SANDER program followed by 10.0 ns MD simulation at constant NPT, which was run using the PMEMD module in Amber10[47] and using the same prescriptions and parameters to those of the former MD simulation. The deformed states were generated by constraining the backbone of the Pro_{21}-Gln_{22}-Gly_{23}-Leu_{24}-Arg_{25}-Gly_{25} segment in the A, B, or C THP chains to a root-mean-squared deviation (rmsd) value of 0 Å from a reference structure taken from a previous MD simulation of the Michaelis complex between the MMP-2 catalytic domain and a decapeptide (Ace-Gly-Pro-Gln-Gly-Ile-Ala-Gly-Gln-Nme; **C1**) mimicking the collagen sequence of chain α1 of collagen type I.[52] With respect to this reference structure, the average structure of the Pro_{21}-Gln_{22}-Gly_{23}-Leu_{24}-Arg_{25}-Gly_{25} backbone in the native A state has an rmsd value of 1.5 Å.

To drive the A(native) → B(distorted) transition smoothly along the targeted MD simulations, we added a harmonic penalty that forces the selected atoms in the sampled structure at a given rmsd from the reference structure using the following equation

$$E = \frac{1}{2}K(\mathrm{rmsd}(t) - \mathrm{rmsd}_0)^2$$

where K stands for the harmonic constant and rmsd_0 is the targeted rmsd value. In our case, 11 intermediate configurations were generated, spanning the range of 1.5 Å separating the A and B structures of fTHP-5. These initial configurations were then used as starting points for umbrella-sampling MD simulations with the rmsd constraint shown above. For each configuration, the force constant for the harmonic constraint was gradually reduced from 500 to 100 kcal/(mol Å^2) in steps of 50 kcal/(mol Å^2) over a period of 0.250 ns of NPT simulation. Each configuration was then sampled with the final constraint of 100 kcal/(mol Å^2) by carrying out a 10 ns NPT MD simulation, from which the last 8 ns were used for data accumulation. All of the targeted simulations were performed using the ABMD code implemented[53] in the SANDER program. Finally, the potential of mean force (PMF) along the rmsd coordinate was constructed by applying the one-dimensional weighted histogram analysis method (WHAM)[54] on data taken at every 0.5 ps of the 8 ns production dynamics.

Docking of the fTHP-5 Molecule within the MMP-2 Active Site. The details of the computational procedure to dock the distorted fTHP-5 molecule within the active site of MMP-2 are as follows. (1) First, we selected 30 equally spaced structures from the last 8.0 ns of each targeted MD simulations of fTHP-5 with partially distorted A/B/C chains in the vicinity of the scissile bond and having an intermediate rmsd value of 0.60 Å with respect to the reference structure. Each structure contained both the coordinates of the solute atoms and a 3.0 Å layer of water molecules around the solute. (2) From our previous 20 ns MD study of the Michaelis complex formed between the MMP-2 enzyme and the **C1** peptide,[55] we took 20 snapshots of the solute atoms solvated by a 3.0 Å layer of solvent molecules. (3) Each one of the fTHP-5 structures was docked within the MMP-2 active site by superposing the backbone atoms of the Pro_{21}-Gln_{22}-Gly_{23}-Leu_{24}-Arg_{25}-Gly_{25} segment in one of the A/B/C chains onto their counterpart atoms in the **C1** decapeptide and then removing the **C1** atoms. Only the solute peptide/protein atoms of the ligand/host systems were considered at this stage. Three different sets of MMP-2/fTHP-5 complexes (i.e., **MMP-2/fTHP-5(A)**, **MMP-2/fTHP-5(B)**, and **MMP-2/fTHP-5(C)** were generated, depending on the A/B/C chain of fTHP-5 bound to MMP-2. Each set included 30 × 20 = 600 structures. (4) For every single MMP-2/fTHP-5 model, steric clashes between the MMP-2 and fTHP-5 atoms

were iteratively identified and relaxed. The coordinates of the clashing residues were relaxed by carrying out 1000 conjugate gradient steps followed by 25 ps of MD using the AMBER03 force field and a distance-dependent dielectric constant ($\varepsilon = 4r_{ij}$). A high temperature value (500 K) is used in the restricted MD simulations to promote uphill moves of bulky side chains that can be important for properly relaxing some steric collapses. Once that the loop over all of the steric clashes is completed, the coordinates of the MMP-2 and fTHP-5 residues involved in the steric clashes were simultaneously optimized. (5) The total energy of the partially relaxed MMP-2/fTHP-5 models is not useful to obtain a compensated energetic description because the number and identity of the MMP-2/fTHP-5 residues that are structurally relaxed is different in each model. Hence, we estimated the MMP-2···fTHP-5 binding energy to assess the stability of the models. The required energies were obtained by using the molecular mechanical (MM) Poisson−Boltzmann Surface area (MM−PBSA) approach, which has been applied to perform many classes of approximate binding-energy calculations, including for protein−protein complexes.[56] Hence, we performed single-point MM−PBSA energy calculations using the SANDER program on the MMP-2/fTHP-5 complexes and on the separated MMP-2 and fTHP-5 fragments. These calculations were performed for all of the models using the PBSA program in Amber10 with similar settings to those detailed below for the MM−PB analyses of the MD simulations. (6) The structural quality information of the most stable MMP-2/fTHP-5 models was analyzed by means of the WHAT_CHECK program.[57] Finally, the water molecules from the 3.0 Å solvent layer of the separate MMP-2 and fTHP-5 fragments that did not show any steric clash among protein atoms or other water molecules were included back in the most stable models for setting up the corresponding MD simulations (see below).

MD Simulations of the MMP-2/fTHP-5 Complexes. The two most favorable docking structures that placed the B or C chain of the partially distorted fTHP-5 molecule within the MMP-2 active site were further analyzed by means of MD simulations. The initial structures of the **MMP-2/fTHP-5(B)** and **MMP-2/fTHP-5(C)** models were surrounded by a periodic box of TIP3P water molecules that extended 20 Å from the protein atoms. In addition, three Cl^- counterions were placed to neutralize the systems. This resulted in a total of 4430 protein atoms being solvated by ∼46 000 water molecules. The parm03 version of the all-atom AMBER force field was used to model the system.[40] For the calcium ions, we employed similar settings to those described elsewhere.[58] For the zinc ions, we used a set of MM parameters that have been developed and tested by us in a previous work.[55,59] In particular, for the catalytic Zn_1, a mixed bonded and nonbonded representation was adopted in which the metal ion is linked to the His_{403}−Nε, His_{407}−Nε, and His_{413}−Nε atoms (1CK7 numbering) and the bridging $[Zn-(OH_2)]^{2+}\cdots{}^{-}OOC-Glu_{404}$ water molecule by explicit MM bonds. In contrast, the carbonyl group of the scissile peptide bond in the fTHP-5 molecule that is supposed to be the fifth ligand around Zn_1 is represented by the standard nonbonded parameters. This mixed description allows flexible substrate binding at the apical position of the Zn_1 site.

Energy minimizations and MD simulations were performed with the 2.7 version of the NAMD program.[51] Solvent molecules and Cl^- counterions were initially relaxed by means of energy minimizations and 100 ps of MD. Then, the full systems were minimized and heated gradually to 300 K during 120 ps of MD. Finally, a 100 ns MD simulation was performed for the **MMP-2/fTHP-5(B)** and the **MMP-2/fTHP-5(C)** models with a time step of 2 fs. Harmonic restraints with force constants of 5−20 kcal/(mol Å) were imposed in selected enzyme/substrate distances during the first 12 ns (Ala_{194}−O···N−$Gln_{22}(P_2)$, Ala_{194}−N···O−$Gln_{22}(P_2)$, Zn_1···O−$Gly_{23}(P_1)$, Ala_{192}−O···N−$Leu_{24}(P_1')$, Leu_{191}−N···O−$Leu_{24}(P_1')$, Pro_{423}−O···N−Arg25-(P_2'), and Tyr_{425}−N···O−$Arg_{25}(P_2')$) to allow MMP-2 to relax in the presence of the B or C chain of fTHP-5 within the active site. The SHAKE algorithm was used to constraint all of the R−H bonds, and periodic boundary conditions were applied to simulate a continuous system. A nonbonded cutoff of 10.0 Å was used, whereas the particle-mesh-Ewald (PME) method with a grid spacing of ∼1 Å was employed to include the contributions of long-range interactions. Langevin dynamics was employed to control the temperature (300 K) using a damping factor of 2 ps^{-1}, whereas pressure control (1 atm) employed Berendsen bath coupling. Coordinates were saved every 5 ps, and only the last 70 ns from each trajectory were considered for analysis using the ptraj program included in the Amber10 package and some other specific software developed locally. Clustering analyses were performed using MMTSB-tools.[60]

Construction of the Ternary Complex MMP-2···fTHP-5···MMP-2. From the most likely model of the MMP-2/fTHP-5 complex in which chain B of fTHP-5 occupies the MMP-2 binding site, we constructed a model of a hypothetical ternary complex formed between two catalytic MMP-2 units and one fTHP-5 molecule. This ternary model, which preserves the overall structure and the binding motifs characteristic of the parent MMP-2/fTHP-5 binary complex, includes a second catalytic domain bound to the central region of chain C in fTHP-5, which turned out to be solvent-exposed along the **MMP-2/fTHP-5(B)** simulation.

To build the initial structure of the MMP-2/fTHP-5/MMP-2 complex, we applied a computational protocol that closely resembles that employed to set up the initial binary complexes. First, we carried out targeted MD and PMF calculations on the **MMP-2/fTHP-5(B)** model in which the backbone of the Pro_{21}-Gln_{22}-Gly_{23}-Leu_{24}-Arg_{25}-Gly_{25} segment in the chain C was constrained to different rmsd values from the same reference structure derived from the **MMP-2/C1** simulation. In these calculations, which were started from the snapshot at 50 ns of the **MMP-2/fTHP-5(B)** trajectory, we used the same settings and prescriptions as those that have been described for the isolated fTHP-5 molecule except that data accumulation in the PMF windows extended up to 5 ns.

The details of the computational procedure to dock the MMP-2/fTHP-5 complex within the active site of a second MMP-2 unit were again very similar to those commented above. Thus, we selected 45 equally spaced structures from the last 4.0 ns of the **MMP-2/fTHP-5(B)** targeted MD simulations having an intermediate $rmsd_0$ value of 0.50 Å. The set of selected MMP-2/fTHP-5 structures was then duplicated, creating thus two identical sets: L (ligand) and H (host). Then, each one of the MMP-2/fTHP-5 structures in the L set was docked within the MMP-2 active site of one H structure by superposing the backbone atoms of the Pro_{21}-Gln_{22}-Gly_{23}-Leu_{24}-Arg_{25}-Gly_{25} segment in the distorted C chain onto their counterpart atoms in chain B of fTHP-5 in the H structure followed by removing all of the fTHP-5 atoms in the H structure. In this way, a set of ternary complexes including 45 × 45 = 2025 structures was generated. Subsequently, steric contacts were relaxed, and the docked

dx.doi.org/10.1021/bi401144p | Biochemistry 2013, 52, 8556−8569

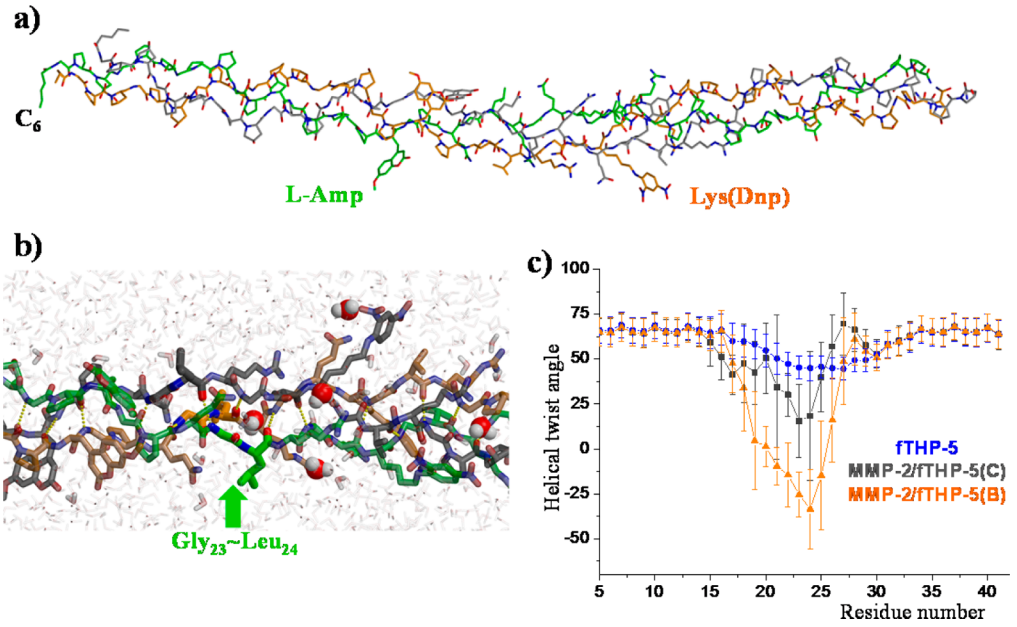

Figure 1. (a) Stick representation of the last snapshot obtained from the 50 ns MD simulation of fTHP-5 in water. Carbon atoms from chains A, B, or C are colored in green, orange, and gray, respectively. (b) Zoomed view around the scissile peptide bond in chain A showing the main interchain H bonds and the position of structural water molecules. (c) Evolution of the average helical twist angle (in degrees) along the sequence of the fTHP-5 molecule in its free state and in complex with the MMP-2 catalytic domain.

complexes were energetically scored by means of the same computational procedure as that used for the binary complexes.

Finally, the most likely MMP-2/fTHP-5/MMP-2 docking model was immersed in a periodic solvent box that extended 20 Å from the protein atoms and extensively relaxed by carrying out a 100 ns MD simulation performed with the NAMD 2.7 program. All of the force-field parameters and the rest of the MD settings were again identical to those employed in the simulations of the MMP-2/fTHP-5 complexes.

Energetic Analyses of the MD Trajectories. To estimate the relative stability of the MMP-2/fTHP-5 models, we computed various free-energy components by performing MM−PB calculations[56,61] over 2000 snapshots extracted from each MD simulation every 100 ps. The snapshots were postprocessed through the removal of all solvent molecules and counterions. The MM−PB energy, which should be interpreted as a physically based scoring function, was computed according to the following equation

$$G_{MM-PB} = E_{MM} + \Delta G_{solv}^{PB} + \Delta G_{solv}^{nonpolar} \quad ([1])$$

where E_{MM} is the molecular mechanics energy, ΔG_{solv}^{PB} is the electrostatic solvation energy obtained from Poisson−Boltzmann calculations,[62] and $\Delta G_{solv}^{nonpolar}$ is the nonpolar part of solvation energy. The latter nonpolar term was estimated by means of two different computational alternatives: (a) $\Delta G_{solv}^{nonpolar} = \Delta H_{solute-solvent}^{vdW} + \gamma MSA$, where $\Delta H_{solute-solvent}^{vdW}$ is the solute−solvent van der Waals energy, whereas the cavitation free-energy contribution to the nonpolar solvation energy is determined by a molecular surface area dependent term, and (b) the nonpolar contribution to the solvation free energy is simply estimated by a solvent-accessible surface area (SASA) dependent term, $\Delta G_{solv}^{nonpolar} = a SASA + b$.

The SANDER program included in Amber10 was used to compute (no cutoff) the molecular mechanics energy terms (E_{MM}), whereas the electrostatic contributions to the solvation free energy were determined using the PBSA program also available in Amber10. In the PB calculations, atomic charges and radii were taken from the parm03 representation. The linearized PB equation was solved on a cubic lattice by using an iterative finite-difference method. The cubic lattice had a grid spacing of 0.33 Å, and the points at the boundary of the grid were set to the sum of Debye−Hückel potentials. The van der Waals interaction energies between solute and solvent atoms were determined for a water shell of 12 Å thickness around the solute with no cutoff using SANDER. To estimate the cavitation energy, the surface tension proportionality constant γ was set to 69 cal mol^{-1} Å^{-2}, and the molecular surface area (MSA) was determined using the MOLSURF program included in Amber10, applying Bondi radii for the solute atoms and a water probe radius of 1.4 Å. The default settings in the PBSA program for computing the SASA-dependent $\Delta G_{solv}^{nonpolar}$ were used (a = 7.2 cal mol^{-1} Å^{-2} and b = 0).

RESULTS

Structure and Dynamics of fTHP-5. The fTHP-5 triple helix was built from sequence, as described in the Materials and Methods, and its phase space was sampled in water by means of 50 ns of MD. Taking into account that the simulation did not start from an experimental structure, the different analyses were performed for the last 40 ns of the trajectory to ensure a complete relaxation of the triple helix in solution. Figure 1a displays the last geometry obtained from the simulation, which confirms that the system remains triple helical. This can be further confirmed by analyzing the presence of the characteristic H-bond pattern observed in the crystal structures of other THPs.[20] For instance, we see in Figure 1b and Table S1 that highly abundant Gly−NH···OC−X interchain H bonds between a glycine amino group in one chain and the carbonyl from the X residue in the repeating (Gly−X−Y) triplet from an adjacent chain occurred along the simulation (81−100% of occupancy and 2.9−3.2 Å of average distance between heavy atoms). Additional H-bond contacts are observed in the central region of the fTHP-5 helix

dx.doi.org/10.1021/bi401144p | Biochemistry 2013, 52, 8556−8569

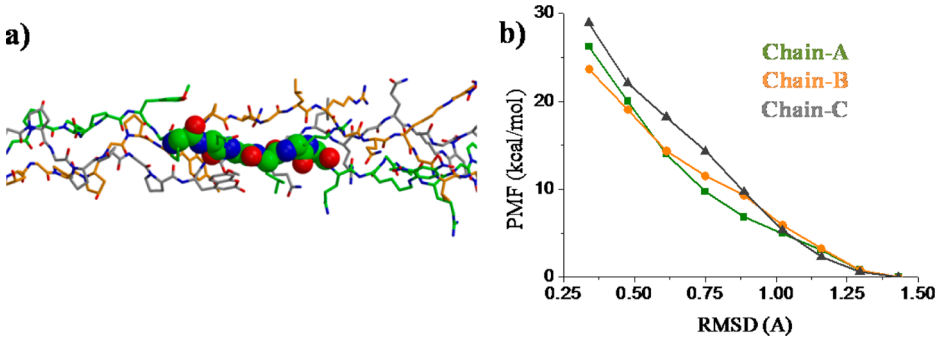

Figure 2. (a) View of a deformed fTHP-5 molecule around the scissile peptide bond in chain A. (b) Free-energy profile along the rmsd coordinate for the deformation of the fTHP-5 chains to approach an extended conformation around the scissile peptide bond.

because of the presence of residues other than proline and hydroxyproline in the X and Y positions of the (Gly−X−Y) triplets, respectively. For instance, less frequent H-bond contacts (58−86% of occupancy) have been characterized between selected side chains and the carbonyl groups from another polypeptide chain (see Table S2). Water also mediates Gly−C═O···(H_2O)···HN−X interchain contacts in the nonprototypical region of fTHP-5 during more than half of the trajectory (68−97% of the simulation time). The rather short average life of these contacts, oscillating between 5 and 16 ps, indicates that water molecules bridging chains are often exchanged. However, even when there is a constant flux of water molecules, the interchain contacts remain rather stable.

THPs are flexible molecules capable of changing (bending) from a linear to a curved (subtly C shape or S shape) structure.[36,63] The overall dynamics of the fTHP-5 molecule can be analyzed by performing a principal component analyses (PCA) of the Cα covariance matrices. The first five PCA modes account for ∼90% of the variance of the backbone Cα atoms (Table S3). These modes can be grouped in three subfamilies representing each a different global movement. Thus, the first two modes, which account for the majority of the structural variability of the triple helix, correspond to the twist/untwist motion of the helix. The second subfamily, constituted in part by the third and by the fourth mode, describes orthogonal bending motions of the whole THP backbone. Finally, the third subfamily corresponds to the fifth mode and describes a zigzag movement of the triple helix.

The helical structure of collagen molecules can be conveniently described by computing the unit twist angle (θ) and the unit height (h) along the triple helix. Following prescriptions described elsewhere,[36] we averaged the θ and h data for the nonprototypical triplets located in the central region of the helix (from Gly_{17} to Arg_{31}) during the last 40 ns of the fTHP-5 trajectory. Interestingly, the resulting values (θ = 52 ± 7° and h = 9.0 ± 0.2 Å) are in between those calculated from previous simulations of a prototypical THP (POG10: θ = 64 ± 1° and h = 8.8 ± 0.2 Å) and of a triple helix whose central region mimics a fragment from type III collagen (T3-785: θ = 47 ± 5° and h = 9.1 ± 0.2 Å). This structural result correlates with the stability ordering of these three triple helices in terms of the melting temperature: 41 °C for fTHP-5, 60 °C for the prototypical helix, and 25 °C for the last one.[23,64] We have also analyzed the variation of the twist angles along the sequence of the fTHP-5 molecule. In Figure 1c we see that the twist angle fluctuates between 60−70° for all the residues in both $(Gly−Pro−Hyd)_5$ extremes, whereas θ ranges between 45° and 60° in the central region. Thus, the twist angle deviates from the standard (prototypical) behavior because of the lack of Pro and Hyp residues occupying the X and Y positions of the (Gly−X−Y) triplet, respectively. In addition it is also clear that the triple helix is partially unwound around the scissile peptide bond as compared with the (Gly−Pro−Hyd) regions.

Deformation of fTHP-5: Targeted MD Simulations and PMF Calculations. To gain knowledge on the structural response of fTHP-5 when the central region of its triple-helical structure is slightly distorted as well as to estimate the associated energetic penalty, we carried out targeted MD simulations and PMF calculations for the conversion of each one of the A/B/C chains in the relaxed fTHP-5 structure into a locally constrained form in which the backbone atoms of the Pro_{21}-Gln_{22}-Gly_{23}-Leu_{24}-Arg_{25}-Gly_{25} residues adopt an stretched conformation more prone to fit along the MMP-2 binding crevice. As mentioned in the Materials and Methods, the reference structure for independently distorting each one of the three fTHP-5 chains was taken from a previous simulation in which the **C1** decapeptide binds to MMP-2 in an extended conformation that is stabilized by H-bond contacts connecting the important backbone positions in the β4 strand and the Ω loop of the enzyme with the corresponding backbone amide groups of the peptidic substrate.

Figure 2a shows a characteristic snapshot from one of the targeted MD simulations corresponding to a reference $rmsd_0$ value of 0.60 Å with respect to the distorted form. Inspection of this model and the various structural analyses (H-bond interchain contacts, helical parameters) confirm that the deformation induced around the Gly_{23}−Leu_{24} bond in chain A hardly alters the global structure of the triple helix. We also found that the relative weight and dynamical features of the most important PCA modes along the targeted MD trajectory closely resemble those of the unrestrained MD simulation. The only remarkable change is the loss of two of the characteristic interchain H bonds, namely, the Gly_{23}−NH···O−Pro_{21} and Gly_{20}−NH···O−Pro_{21} interactions between the A···B and C···A chains that are replaced in the distorted fTHP-5 state by H-bond contacts with water molecules and an alternative Gly_{20}−NH···O−Gln_{22} interaction, respectively. Similar structural observations were carried out in the other two targeted MD simulations aimed to distort chains B or C.

Even though the backbone rearrangement in the vicinity of the Gly_{23}−Leu_{24} linkage resulted in small and well-localized structural changes of the fTHP-5 molecules, the energetic impact of the geometric constraint turned out to be quite significant regardless of the A/B/C chain being distorted, as shown by the calculated free-energy profiles along the rmsd coordinate (Figure 2b). Thus, free energy increases steadily

dx.doi.org/10.1021/bi401144p | Biochemistry 2013, 52, 8556−8569

from the relaxed structure at rmsd ~1.5 Å to the more extended chains at low rmsd values. Integration of the PMF profiles within the 0.4−1.5 rmsd interval allows us to obtain the following estimations of the free-energy change required to deform the fTHP-5 structure: 9.9, 10.4, and 11.8 kcal/mol for the A/B/C chains, respectively. Moreover, the population of fTHP-5 structures having rmsd values with respect to the reference (extended) conformation below 0.25 Å was very scarce all along the targeted MD simulations in spite of the relatively large harmonic constraints that were applied (~4 kcal mol^{-1} $Å^{-2}$ per atom). Hence, these results suggest that the local unwind of the fTHP-5 triple helix prior to substrate binding within the active site and catalysis could be a major contribution to the overall free-energy cost of MMP-2-assisted hydrolysis. This effect could be due to the disruption of the characteristic H-bond pattern of the triple helix occurring upon the distortion of the backbone conformation, which in turn may affect the efficiency of the intramolecular dipole−dipole alignment and solvent stabilization of the triple-helical structure.

Construction and Validation of the MMP-2/fTHP-5 Models: Docking Calculations, MD Simulations, and Energetic Analyses. Our automated docking protocol produced a total of 1800 initial complexes by superposing a set of relaxed structures of the MMP-2 catalytic domain in complex with the **C1** peptide, which were generated by a former MD simulation, onto the locally deformed fTHP-5 structures extracted from the three targeted MD simulations. Steric clashes between the MMP-2 and fTHP-5 atoms were partially relaxed through a combination of constrained energy minimizations and short MD simulations, and, finally, the quality of the docked structures was reassessed by MM−PB energy calculations and by counting the remaining bad contacts. However, the ratio of docked structures that had few or no serious steric collapses was rather low, which was not entirely unexpected given that the employed fTHP-5 structures largely retained their compact and bulky triple-helical arrangement. As a matter of fact, 90% of the MMP-2/fTHP-5 docked structures in which chain A of the substrate molecule was occupying the binding site presented ample interprotein overlaps that prevented any further model-building operation, whereas the local relaxation of the remaining 10% of structures scored very poorly in terms of the final MM−PB binding energies (i.e., positive values of thousands of kilocalories per mole) and the abundance of bad contacts. However, the same computational protocol was able to partially relax >96% of the docked structures when chains B and C were placed within the MMP-2 binding crevice. Moreover, visual inspection of the 3 or 4 most stable models, which had relatively low binding energies of a few tens or hundreds of kilocalories per mole and only a handful of bad contacts, confirmed that they were reasonable structures for subsequent model-building operations. Thus, the most stable docking models for the **MMP-2/fTHP-5(B)** and **MMP-2/fTHP-5(C)** complexes were then analyzed by the WHAT_CHECK program, which detected wrong conformations for two and three protein side chains, respectively. These problems were corrected manually, and the side chains were relaxed again through constrained minimizations.

Although the semiflexible docking calculations generated two models for the interaction of the catalytic domain of MMP-2 with the slightly deformed fTHP-5 molecule, it is clear that, owing to the size and complexity of the fTHP-5 substrate, further relaxation of the models by means of extended MD simulations was necessary to assess better the nature and importance of the interprotein interactions. Moreover, the possible rearrangement of the MMP-2 enzyme in response to the presence of the triple helix or the role played by specific water molecules mediating the enzyme/substrate interaction are neglected in these docking analyses. In addition, they cannot provide insight into the dynamical behavior of the helix bound to the enzyme. To explore these and other relevant issues related with the placement of the triple helix within the MMP-2 active site, we performed 100 ns MD simulations of the two most favored MMP-2/fTHP-5 docked structures in aqueous solution.

The time evolution of the rmsd values along the MD simulations with respect to the 1CK7 crystal structure indicates that the structure of the MMP-2 catalytic domain is well-equilibrated in the two simulations (Figure S2 in the Supporting Information). The same plots show a transition in the global MMP-2 structure after 30 ns in the **MMP-2/fTHP-5(C)** configuration, and, accordingly, only the last 70 ns were analyzed in each trajectory. The average rmsd values, 1.8 ± 0.1 Å for the backbone atoms without including the N-terminal fragment, suggest that the structure of the catalytic domain of the enzyme is not significantly distorted in the presence of the THP molecule. This is fully confirmed by the superposition of the average structures of the MMP-2 catalytic domain onto the 1CK7 crystal structure. The largest shift arises at the N-terminal coil, which was positioned in the superactivated conformation in our simulations, and in the characteristic S (or Ca/Zn) and Ω loops that contact the fTHP-5 molecule (see Figure S3).

The MD simulations started at the docked models reveal that the triple helix of fTHP-5 is largely distorted in its central region to achieve a proper binding to the MMP-2 active site, which seems to be somewhat in contrast with the small structural changes experienced by MMP-2. Thus, the evolution of the helical twist angle against sequence averaged for the three α chains in the bound fTHP-5 molecule (Figure 1c) clearly shows that the triple helix is unfolded in the central region around the scissile peptide bond (Gly_{23}−Leu_{24}) in the two MMP-2/fTHP-5 complexes. Moreover, the unfolding is much more pronounced when chain B binds within the MMP-2 active site (the average helical twist angle becomes negative at the central region). To analyze further the changes in the triple helix associated to its binding to MMP-2, we also determined the percentage of occurrence and the average interatomic distance of the Gly−NH···O−X H bonds that characterize the triple-helical structure. The notable rearrangement of chains B or C upon substrate binding results in the weakening and/or the removal of several interchain H bonds in the area (see Table S1). Although some Gly−NH···O−X contacts remain mediated by water molecules, the characteristic H-bond pattern of the triple-helical structure is clearly lost in the central region of the fTHP-5 molecule.

To analyze the global dynamics of the partially unfolded fTHP-5 molecule bound to MMP-2, we performed clustering analyses of the substrate conformations by grouping them into clusters by considering the rmsd values of the backbone Cα atoms. Figure 3a displays the cluster representatives obtained for the **MMP-2/fTHP-5(B)** and the **MMP-2/fTHP-5(C)** simulations. Comparison of the clustering results confirms that the fTHP-5 molecule is globally more flexible when chain B is located in the MMP-2 active site. The different clusters mainly arise because of the movement of the prototypical terminal fragments of fTHP-5 that maintain their triple-helix conformation all along the simulations. In contrast, the central

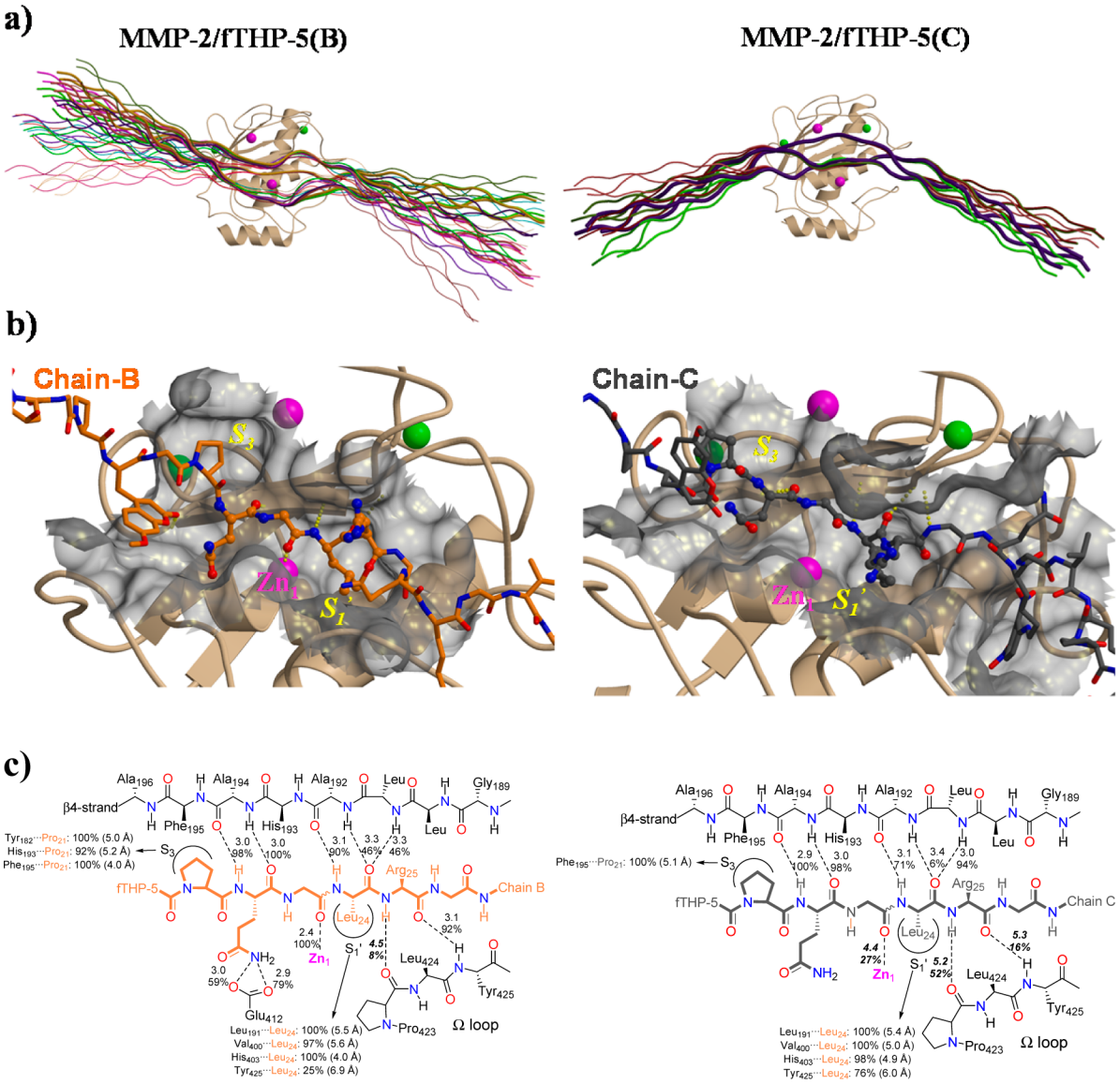

Figure 3. (a) Ribbon models of the MMP-2 catalytic domain in complex with fTHP-5. For fTHP-5, the centroids determined by the clustering analyses are shown with a thickness proportional to their relative weight. (b) View of the MMP-2 active site in complex with chain B or chain C of fTHP-5. For clarity, the other fTHP-5 chains are not represented. (c) Schematic representation of the most important MMP-2···fTHP-5 interactions.

region of the fTHP-5 molecule that interacts with the catalytic domain of the enzyme is best described by segments of extended coils in all of the clusters. In addition, Figure 3a also shows that the MMP-bound fTHP-5 molecule is considerably bent and that the relative orientation between the curved fTHP-5 with respect to the MMP-2 catalytic domain depends on the identity of the chain (B or C) being located within the active site.

Concerning the direct contacts between fTHP-5 and MMP-2, our structural analyses indicate that fTHP-5 binds through a series of polar and hydrophobic contacts in a similar fashion to that of small peptide molecules (Figure 3b,c). Most of the enzyme/substrate contacts involve the triple helix chain that is placed within the active site of the enzyme and sites S_3–S_3' of the catalytic domain. For instance, we observed in the two simulations highly persistent Ala_{194}–NH···O–Gln_{22} and Gln_{22}–NH···O–Ala_{194} contacts at S_2 with the simultaneous placement of the Leu_{24} side chain within the S_1' hydrophobic pocket. However, there are also noticeable differences in some of the MMP-2/fTHP-5 contacts depending on which fTHP-5 chain (B or C) is aligned in the active-site groove. Thus, at the scissile peptide bond, the Gly_{23} carbonyl group of fTHP-5 (P_1) remains coordinated to the catalytic zinc ion during 100% of the **MMP-2/fTHP-5(B)** simulation, but this contact is weakened and becomes mediated by water molecules along the **MMP-2/fTHP-5(C)** trajectory. This change slightly increases the distance between the nucleophile (Zn_1-coordinated water molecule) and the carbonyl group of the scissile peptide bond from 2.9 ± 0.1 Å for **MMP-2/fTHP-5(B)** to 3.3 ± 0.2 Å for **MMP-2/fTHP-5(C)**. There are also significant differences in the occupation of the S_3 hydrophobic pocket built by the side chains of Tyr_{182}, His_{193}, and Phe_{189}. As expected, the P_3 Pro_{21} from chain B is buried within the S_3 pocket in the **MMP-2/fTHP-5(B)** model. In contrast, residues Pro_{21} and Leu_{24} from chain B together with Pro_{21} from chain C interact with the S_3 residues in the **MMP-2/fTHP-5(C)** simulation. Overall, we conclude that the **MMP-2/fTHP-5(B)** configuration results in

dx.doi.org/10.1021/bi401144p | *Biochemistry* 2013, 52, 8556–8569

Table 1. Average Values for the MM−PB Energy Components (in kcal/mol) for the Various MD Trajectories Examined in This Work[a]

	$\overline{E}^{MM}_{gas}$	$\Delta\overline{G}^{PB\ b}_{solv}$	$\Delta\overline{G}^{nonpolar}_{solv}$	$\overline{G}^{MM-PB}$
MMP-2/fTHP-5(chain-B)	−324.1 (2.7)	−2885.3 (2.3)	120.4 (0.1) *151.6 (0.8)*[b]	−3087.2 (1.4) *−3056.0 (1.6)*[b]
MMP-2	−1262.3 (2.7)	−2022.8 (2.4)	64.9 (0.1)	−3220.2 (1.0)
fTHP-5	1487.5 (2.1)	−1311.2 (0.5)	73.2 (0.1)	249.5 (0.8)
interaction energy	−549.4 (0.7)	448.8 (0.6)	−17.7 (0.1)	−118.3 (0.2)
MMP-2/fTHP-5(chain-C)	−229.7 (2.5)	−2916.1 (2.0)	118.3 (0.1) *155.8 (0.8)*[b]	−3025.7 (1.4) *−2988.2 (1.6)*[b]
MMP-2	−1159.1 (2.2)	−2080.5 (1.8)	67.9 (0.0)	−3171.8 (1.1)
fTHP-5	1480.2 (1.0)	−1294.3 (0.6)	72.6 (0.1)	258.4 (0.8)
interaction energy	−550.8 (0.8)	458.8 (0.7)	−22.2 (0.1)	−114.2 (0.3)
isolated fTHP-5	1455.9 (1.4)	−1336.2 (0.7)	72.0 (0.1)	193.6 (1.2)
MMP-2/fTHP-5(B,C)/MMP-2	−1809.6 (2.9)	−4654.9 (2.3)	166.8 (0.4) *359.1 (1.0)*[b]	−6297.7 (1.7) *−6105.4 (2.0)*[b]
MMP-2[1]	−1166.0 (1.9)	−2096.8 (1.5)	65.8 (0.0)	−3197.0 (1.1)
fTHP-5	1578.8 (0.9)	−1374.9 (0.5)	75.9 (0.1)	279.1 (0.7)
MMP-2[2]	−1205.4 (2.0)	−1989.0 (1.6)	67.2 (0.0)	−3127.2 (1.7)
interaction energy MMP-2···fTHP5···MMP-2	−1017.3 (1.3)	802.9 (1.0)	−41.1 (1.2)	−255.5 (0.5)

[a]Standard errors of the mean values are indicated in parentheses. Interaction energies for the MMP-2/fTHP-5 complexes were obtained using the one-trajectory approximation. The MM−PB calculations were done using snapshots from the last 70 (MMP-2/fTHP-5 complexes) or 40 ns (fTHP-5). [b]Data that include the vdW interaction energy between the solute and water molecules (i.e., $\Delta G^{nonpolar}_{solv} = \Delta H^{vdW}_{solute-solvent} + \gamma A$) are given in italics.

more stable MMP-2···fTHP-5 contacts favorable for substrate binding and catalysis.

To investigate the relative stability of the MMP-2/fTHP-5 configurations, we evaluated their approximate free energy (G_{MMPB}) in aqueous solution as described in the Materials and Methods. First, we plotted the evolution of the G_{MMPB} values (including the vdW interaction between solute and explicit waters) along the MD trajectories to make sure that they were reasonably equilibrated and fluctuated smoothly during the last 70 or 40 ns of the simulation time (Figure S4 in the Supporting Information). Then, the mean values for the various energetic terms that are combined into the MM−PB scoring function were computed (Table 1).

From the G_{MMPB} data in Table 1, the relative stability of the two models can be assessed directly. Thus, it turns out that binding of fTHP-5 to the MMP-2 catalytic unit through chain B is energetically much more favorable than binding through chain C by 68 kcal/mol in terms of G_{MMPB} with solute−water vdW interactions. The same energy difference amounts to 62 kcal/mol when the simpler SASA term is used to estimate the nonpolar solvation. Although the MM−PB method used in this work can be considered as a physically based scoring function, it predicts neither highly accurate free-energy differences nor absolute binding energies because of limited sampling, the inclusion of solvent continuum, and, perhaps most importantly, the neglect of the solute configurational entropy. However, the large magnitude of the observed G_{MMPB} differences and their relatively low statistical uncertainty suggest that we can safely assign the **MMP-2/fTHP-5(B)** configuration as the most likely model for representing the MMP-2/fTHP-5 complex.

Table 1 also collects the mean MMPB energies of the MMP2 and fTHP-5 molecules (including now only the SASA nonpolar contribution) that were computed using coordinates extracted from the MD simulations of the MMP-2/fTHP-5 complexes and fTHP-5. On the basis of these data, we see that the larger stability of **MMP-2/fTHP-5(B)** stems mainly from the lower energetic distortion suffered by the MMP-2 catalytic domain upon substrate binding. In effect, the average MM−PB energies of fTHP-5 in the **MMP-2/fTHP-5(B)** and **MMP-2/fTHP-5(C)** trajectories are similar, 249 and 258 kcal/mol, respectively, more than 55 kcal/mol above that for the relaxed fTHP-5 molecule. Similarly, the equivalent MMP-2···fTHP-5 interaction energies that must compensate for the fragment deformation have values of −118 and −114 kcal/mol. In contrast, the MM−PB destabilization of the MMP-2 moiety is about 50 kcal/mol larger in **MMP-2/fTHP-5(C)**. These observations seem to be consistent with the results of the structural analyses that show that the S and Ω loops present larger deviations with respect to the reference X-ray structure in the **MMP-2/fTHP-5(C)** configuration.

Ternary Complex MMP-2···fTHP-5···MMP-2. Apart from vdW contacts between the side chain of Leu_{24} in fTHP-5 chain C and some solvent-oriented Ω-loop residues of MMP-2, the central segment of chain C exhibits an unwound and solvent-accessible conformation during the **MMP-2/fTHP-5(B)** simulation. Hence, the question that naturally arises is whether or not the structure of the binary MMP-2/fTHP-5 complex is compatible with the binding of a second catalytic unit that could anchor chain C of fTHP-5. To build a model of this hypothetical complex and to assess further its feasibility, we resorted to the same methodology that was used for the binary complexes. Thus, we performed first targeted MD simulations and PMF calculations on the **MMP-2/fTHP-5(B)** configuration that were aimed to force the central residues of chain C in fTHP-5 to approach the conformation of the MMP-bound **C1** peptide substrate. These preliminary calculations showed that although the Pro_{21}-Gln_{22}-Gly_{23}-Leu_{24}-Arg_{25}-Gly_{25} residues in chain C had already lost their helical structure in the **MMP-2/fTHP-5(B)** complex, the energetic cost of constraining their backbone atoms is still significant. Thus, the estimated free-energy change from the integration of the PMF profile within the 0.5−1.8 rmsd interval amounts to 4.9 kcal/mol, which is ∼5 kcal/mol below the free energy for the equivalent deformation of the isolated fTHP-5 molecule. In addition, these simulations provided suitable structures for carrying out the semiflexible protein−protein docking calculations, which in turn rendered a set of ternary complexes that had very few or no steric clashes.

dx.doi.org/10.1021/bi401144p | *Biochemistry* 2013, 52, 8556−8569

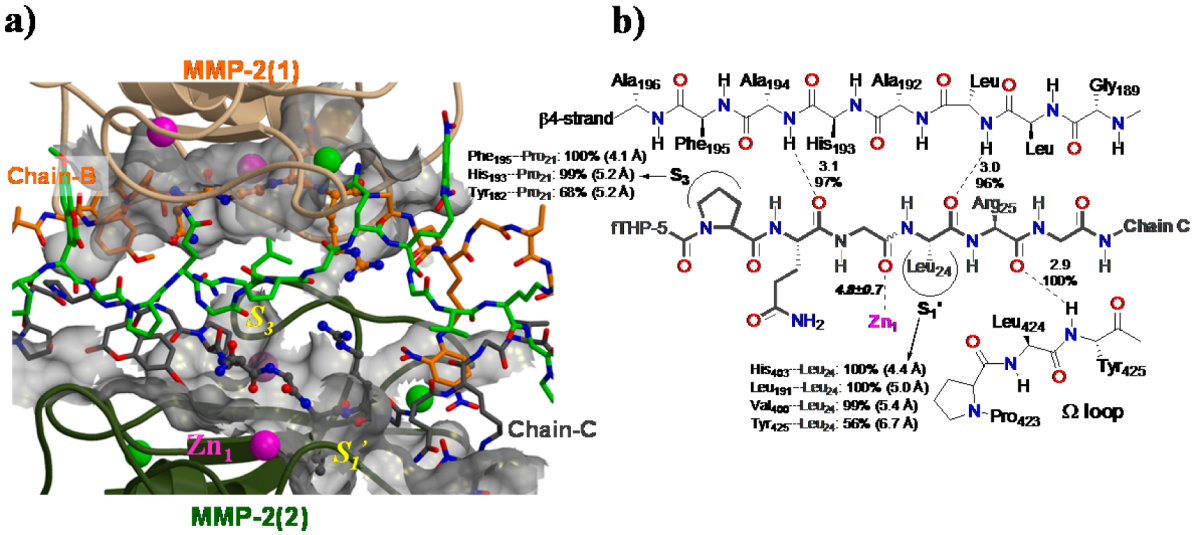

Figure 4. (a) View of the ternary complex formed between two MMP-2 catalytic domains and one fTHP-5 molecule. (b) Schematic representation of the most important MMP-2···fTHP-5 interactions involving the second MMP-2 unit and chain C of fTHP-5.

For the sake of brevity, we focus now on the presentation of the most remarkable features of the **MMP-2/fTHP-5(B,C)/MMP-2** model that was relaxed by a 100 ns MD simulation started at the most stable docked structure. Concerning the overall structure of the two MMP-2 catalytic domains, the rmsd plots indicate that the first domain is well-equilibrated all along the simulation, having an average rmsd of 2.5 ± 0.1 Å (1.8 ± 0.1 Å for backbone atoms), whereas the second domain, which binds to chain C of fTHP-5, suffers a structural transition around 20 ns and thereafter its rmsd fluctuates at higher values: 2.9 ± 0.1 and 2.3 ± 0.1 Å for all-heavy atoms and backbone atoms, respectively. The larger departure of the second MMP-2 unit from the reference structure is mainly due to the rearrangement of the $\beta3-\beta4$ and Ω loops as well as the $\beta3$-sheet residues. Visual inspection of MD snapshots suggests that these structural rearrangements can be induced by unfavorable contacts with the bulky side chains of the nonstandard Dnp_{27} residues in chains B and C. The two MMP-2 units only establish a few polar and vdW interactions among residues belonging to the Ω loop of the first MMP-2 unit and the $\beta3-\beta4$ loop of the second one (e.g., Gln_{132}–C═O···H–Nδ–His_{69} and Pro_{140}···Pro_{74}; these interactions are >10 Å beyond the Zn_1 sites). However, we found again that the triple-helical conformation of fTHP-5 is completely lost in its central region but remains unaltered at the two ends comprising the prototypical $-(Gly-Pro-Hyp)_3-$ triplets.

Figure 4 displays a close view of a representative MD snapshot of the **MMP-2/fTHP-5/MMP-2** complex, which illustrates the placement of the B and C fTHP-5 chains into the two different binding pockets. On one hand, the polar and hydrophobic interactions between the chain-B residues and the first MMP-2 catalytic domain observed during the MD simulation closely reproduce those that were characterized for the binary complex, both in terms of the identity of the involved residues and in terms of their relative abundance (Figure 3). On the other hand, chain C and the second MMP-2 unit give similar contacts as shown in Figure 4b. For example, the Pro_{21} ring and Leu_{24} side chain lie within the S_3 and S_1' hydrophobic pockets all along the MD simulation, whereas the backbone carbonyl groups of Gly_{23} (P_1) and Leu_{24} (P_1') form H-bond interactions with the backbone amide groups alongside the $\beta4$ sheet. However, the overall fitting of chain C to the second MMP-2 binding crevice is less optimal than that between chain B and the first MMP-2 unit because the chain-C residues form fewer H-bond contacts and the corresponding catalytically important Zn1···O═C–Gly_{23} interaction is rather weak (Figures 3 and 4).

Table 1 also collects the results of the MM–PB energetic analyses carried out on the **MMP-2/fTHP-5/MMP-2** trajectory. As in the case of the binary complexes, we observed first that the MM–PB free-energy components were well-equilibrated and fluctuated around its mean value during the last 70 ns. Consistent with the geometrical analyses, the comparison of the mean G_{MM-PB} for the separated MMP-2 units shows that the second MMP-2 unit is destabilized by ∼70 kcal/mol with respect to the first one. Similarly, the energetic penalty for the distortion of the fTHP-5 substrate in the ternary complex increases by ∼30 kcal/mol with respect to the G_{MM-PB} values observed in the binary complexes. However, the MM–PB estimations for the interaction energy among the three protein fragments, −255 kcal/mol, is ∼137 kcal/mol below that of the parent **MMP-2/fTHP-5(B)** complex. Therefore, on the basis of the present MM–PB analyses, the larger distortion of the MMP-2 and THP fragments could be compensated for by the stronger protein–protein interactions, and, consequently, formation of the ternary complex cannot be ruled out. Nevertheless, it is also clear that the computation of absolute free energies of binding, which is an extremely challenging computational and theoretical task, would be necessary to assess better the stability of the hypothetical ternary complexes.

DISCUSSION

As mentioned in ealier, THP molecules have been useful models to understand triple-helix structure and stability as well as to investigate the interaction of collagens with extracellular matrix proteins like the MMPs. In addition, they have been proposed as interesting biomaterials for future applications. However, very limited structural information is available for most of the triple helices synthetized to date. This knowledge gap can be filled by molecular simulations. Thus, starting from the amino acid sequence it is possible to build a triple-helix model for fTHP-5 (a synthetic collagen II model) that can be further explored and validated through an extensive MD

dx.doi.org/10.1021/bi401144p | Biochemistry 2013, 52, 8556–8569

simulation in explicit solvent (provided that appropriate parameters are derived for the nonstandard residues). In fact, the MD simulation characterizes in detail the structure and dynamics in aqueous solution of fTHP-5. We observed that the triple helix remained stable during all of the simulation time, which is in agreement with the melting temperature (T_m ~41 °C) measured for this THP.[23] However, the simulation also points out that the triple helix is far from being rigid, undergoing frequent and ample twist/untwist and bending movements that are characterized by the PCA analysis. Compared with the prototypical terminal fragments, the central region of fTHP-5 is slightly unwound with interchain H bonds mediated by exchangeable water molecules. This partial loss of the helical character around the scissile peptide bond, also observed for other THPs,[65] is supposed to be important for the hydrolytic activity performed by enzymes like the MMPs.[9,66,67]

The collagen triple helix has to locally unwind prior to hydrolysis because only one chain can be accommodated within the narrow active site of the MMP enzymes. Similarly, it is commonly assumed that peptide substrates align in an extended fashion by establishing a number of polar and hydrophobic interactions with the so-called S_3−S_3' sites of the enzyme. To evaluate the structural and energy impact associated to the distortion of one chain of the fTHP5 molecule (A, B, or C) to adopt a peptidelike configuration more suited for MMP binding, we performed three independent series of targeted MD simulations and PMF calculations. Curiously, the structural analyses of the constrained simulations revealed that in the absence of MMPs the deformation induced around the scissile peptide bond has only a minor and localized effect that does not modify the global structure of the triple helix. The energy penalty for the local unfolding around the $Gly_{23}(P_1)$−$Leu_{24}(P_1')$ peptide bond in chain A, B, or C of fTHP-5 is estimated to be around 10 kcal/mol regardless of the peptide chain, which shows that none of them has an intrinsic preference to be the first one hydrolyzed in the active site of the MMPs. Although the PMF calculations were carried out in the absence of the MMP-2 enzyme, they suggest that fTHP-5 unwinding should be a significant contribution to the overall energy barrier for the MMP-assisted hydrolytic process.[23] However, we also note that previous PMF calculations performed on a 45-residue model of collagen type I lacking the prototypical triplets characteristic of fTHP-5 and kinetic analyses of collagen I degradation indicate that partially unfolded vulnerable states could be energetically accessible to some triple helices in their native states.[66,68]

The interaction between the ubiquitous MMP-2 enzyme and the locally deformed fTHP-5 molecule was first analyzed by semirigid docking calculations that place chain A, B, or C within the active site. Because the three identical chains in the fTHP-5 molecule intertwine and are staggered by one residue to form a right-handed triple helix, the scissile peptide bonds are not placed in an equivalent position within the tridimensional structure of the helix[14] so that the MMPs can discriminate among them a priori. This seems to be the case with the MMP-2/fTHP-5 complex because the docking analyses predict that the MMP-2 catalytic domain cannot bind and hydrolyze chain A of the fTHP-5 triple helix in the first place. However, the most stable docked MMP-2/fTHP-5 complexes with chain B or chain C placed in the enzyme active site, which were built from snapshots of the targeted MD simulations of fTHP-5, retain most of the helical character in the central region of the substrate and suggest that the MMP-2 binding crevice can recognize triple-helical motifs. Nevertheless, these docked structures needed to be relaxed by extended MD simulations not only to optimize the MMP-2···fTHP-5 interactions but also to determine the actual conformation of the fTHP-5 molecule. As a matter of fact, the triple-helix conformation is completely lost around the scissile peptide bond during both the **MMP-2/fTHP-5(B)** and **MMP-2/fTHP-5(C)** simulations, showing that MMP···THP interactions play a key role in the unwinding process of THP during the MMP-assisted hydrolysis. Interestingly, these enzyme−substrate active-site contacts seem compatible with the crystal structure obtained for the MMP-12 enzyme in complex with two short peptides mimicking the position of the two products of the hydrolysis reaction of a single peptide chain.[69] In particular, the interactions with the peptide bound within the primed side of the active site (Leu_{181}−N···O−Pep(P_1') 2.9 Å, P_1' side chain within the S_1' pocket, Pro_{238}−O···N−Pep(P_2'), Tyr_{240}−N···O−Pep(P_2')) are well-reproduced by our simulations.

The energetic analyses of the trajectories suggest that the MMP···THP interactions could partially compensate for the THP distortion penalty. In this respect, it is interesting to note that several experimental studies point out that the unwinding of the triple helix is the rate-determining step during proteolysis. Thus, the hydrolysis of different fluorogenic THPs by MMP-1 and MMP-14 shows that an increase in the thermal stability of the substrate decreases the ability of the enzymes to cleave it.[27] In addition, kinetic studies on the hydrolysis of two isoforms (homotrimer and heterotrimer) of type I collagen performed by MMP-1 has been seen to be compatible with a mechanism in which the enzyme stochastically promotes the unwinding of the triple helix as the rate-determining step.[70] Finally, the application of an extensional force over a collagen type I molecule, which presumably unwinds the triple helix, increases the proteolysis rate catalyzed by MMP-1.[71]

Besides unraveling the unwound conformation of the MMP-bound THP substrate, the geometrical and energetic analyses of the MMP-2/fTHP-5 simulations have produced further information concerning their structural features and binding preferences. Most remarkably, the simulations revealed that the two configurations are not equivalent and support the assignation of the **MMP-2/fTHP-5(B)** model with the central chain of the fTHP-5 molecule bound within the MMP-2 active site as the most likely one. Earlier experimental evidence obtained for other MMPs are consistent with our computational results. Thus, an inspection of the product distribution, as monitored by HPLC in the time course of the MMP-1 or MMP-13 digestion of a THP model of collagen I assembled in the $\alpha1\alpha2\alpha1$ register, has been interpreted by considering that the $\alpha2$ chain is the first one to be cleaved.[72] In another work, it has been observed that the Glu_{200}Ala mutant of MMP-1 resulted in a catalytically inactive enzyme that is able to unwind the triple helix of collagen I. In the presence of this mutant, noncollagenolytic proteinases can hydrolyze the $\alpha1$(I) chain of collagen I more rapidly than the active MMP-1 alone, but this effect of the mutant enzyme is not observed when an inhibitor is bound within the active site. The authors interpreted these results by considering that MMP-1 preferentially interacts with the $\alpha2$(I) chain of the triple helix and that this would be the chain to be cleaved in the first place.[9] In the case of MMP-2, catalytic parameters (K_m and k_{cat}) for the enzymatic cleavage of collagen I pointed to the $\alpha2$ chain as the first to be hydrolyzed.[73] Taking into account that collagen I is supposed to be assembled in an $\alpha1\alpha2\alpha1$ register,[74] we propose that the

dx.doi.org/10.1021/bi401144p | Biochemistry 2013, 52, 8556−8569

first collagen chain to be cleaved would be positioned in the MMPs similarly to that of the B chain in our **MMP-2/fTHP-5(B)** model.

Another interesting feature of the **MMP-2/fTHP-5(B)** model is that the MMP-2 catalytic domain is not significantly distorted. In contrast, the fTHP-5 triple helix is completely unwound in the central region that contacts the MMP-2 residues, and the whole THP molecule adopts a curved configuration that retains a significant mobility at the prototypical N- and C-terminal fragments. This global arrangement of the bound triple helix resembles that observed in single-molecule images obtained for the interaction of MMP-9 with collagen II fragments by atomic force microscopy experiments.[10] It is also compatible with an undisturbed triple-helical structure at the N and C ends constituted by prototypical collagen triplets. This observation is in agreement with experimental evidence obtained by measuring the melting temperature of collagen I in the presence of hydrolytically inactive MMP-1, which showed that although collagen is partially unwound through its interaction with the inactive MMP-1 it retains its triple-helical character.[9] However, it may be worth noting again that the enzyme−substrate contacts characterized when chain B is placed within the MMP-2 active site are well-suited for the hydrolysis of the scissile peptide bond by the Zn-bound water molecule assisted by the conserved glutamic acid.[75]

According to high-performance liquid chromatography experiments, MMP-2 degrades triple-helical substrates with the release of partially digested intermediates in which a cut through only one or two strands is detected.[28] These intermediate species in the hydrolysis of a THP could result from the interaction of the same substrate molecule with one or two MMP-2 enzymes. The binding of several collagenases to the same triple helix has been previously considered in the formulation of a phenomenological "Brownian ratchet" model that reproduces the key features of the experimental observations by two-photon excitation fluorescence correlation spectroscopy of the interaction of MMP-1 enzymes with a collagen fibril.[19] In this work, we found that such molecular association, in a catalytically competent fashion, can be accessible when two isolated MMP-2 catalytic domains interact with the B and C chains of a THP substrate, respectively. Thus, the docking calculations followed by MD analyses point out that ternary **MMP-2/fTHP-5(B,C)/MMP-2** can be structurally and energetically feasible, although the second catalytic unit bound to the C chain exhibits a larger distortion and worse enzyme/substrate contacts. Nonetheless, the stability of these ternary complexes and their potential relevance may also depend on the structure of other THP or collagen substrates as well as the presence of the rest of the MMP-2 domains.

In summary, the application of a broad array of computational methods together with the experience and results gained in previous simulations performed on simpler MMP-2 and/or THP systems have rendered a realistic molecular model of the prereactive MMP-2/fTHP-5 complex that unravels the most important MMP···THP binding determinants as well as the structural rearrangement induced in the THP substrate by the MMP-2 catalytic domain. Several features of this model (the preference for binding chain B, the global arrangement of the THP molecule, etc.) are nicely in agreement with experimental proposals, which in turn further supports the interest in the model and its ability to complement the experimental observations. Moreover, we believe that the structure of the MMP-2/fTHP-5 complex reported in this work could be a particularly suitable starting point for studying computationally either the molecular pathway leading to the formation of MMP-2/THP complexes or the mode of action of full-length MMPs during their collagenolytic activity.

■ ASSOCIATED CONTENT

Supporting Information

Interchain Gly-NH···O-Pro interactions in the different fTHP-5 simulations. Water-bridged interchain interactions for the native form of fTHP-5. Summary of PCA analyses for the native form of fTHP-5. Plots of the helical twist angle versus residue number for the distorted fTHP-5 and the ternary MMP-2/fTHP-5/MMP-2 complex. Time evolution of the rmsd of the MMP-2 catalytic domain in the different simulations. Superposition of the MMP-2 catalytic domain in the 1CK7 structure and in the average structures from the MD simulations. H-bond analyses of important enzyme−substrate interactions in the MMP-2/fTHP-5 simulations. Segregated rmsd values of the MMP-2 catalytic domain in the different simulations. G_{MMPB} plots along the MD simulations. PDB coordinates of the last snapshot of the **MMP-2/fTHP-5(B)** configuration. This material is available free of charge via the Internet at http://pubs.acs.org.

■ AUTHOR INFORMATION

Corresponding Author

*E-mail: diazfnatalia@uniovi.es. Tel.: +34-985103468. Fax: +34-985103125.

Funding

This research was supported by grant CTQ2007-63266 (MEC, Spain).

Notes

The authors declare no competing financial interest.

■ ACKNOWLEDGMENTS

Part of the simulation work was carried out at the Barcelona Supercomputing Center − Centro Nacional de Supercomputación (BSC−CNS), and we gratefully acknowledge the computer resources, technical expertise, and assistance provided by the BSC−CNS.

■ REFERENCES

(1) Murphy, G., and Nagase, H. (2011) Localizing matrix metalloproteinase activities in the pericellular environment. *FEBS J. 278*, 2−15.

(2) Butler, G. S., and Overall, C. M. (2009) Updated biological roles for matrix metalloproteinases and new "intracellular" substrates revealed by degradomics. *Biochemistry 48*, 10830−10845.

(3) Rodríguez, D., Morrison, C. J., and Overall, C. M. (2009) Matrix metalloproteinases: What do they not do? New substrates and biological roles identified by murine models and proteomics. *Biochim. Biophys. Acta 1803*, 39−54.

(4) Gialeli, C., Theocharis, A. D., and Karamanos, N. K. (2011) Roles of matrix metalloproteinases in cancer progression and their pharmacological targeting. *FEBS J. 278*, 16−27.

(5) Bigg, H. F., and Rowan, A. D. (2001) The inhibition of metalloproteinases as a therapeutic target in rheumatoid arthritis and osteoarthritis. *Curr. Opin. Pharmacol. 1*, 314−320.

(6) Korpos, E., Wu, C., and Sorokin, L. (2009) Multiple roles of the extracellular matrix in inflammation. *Curr. Pharm. Des. 15*, 1349−1357.

(7) Denys, H., Braems, G., Lambein, K., Pauwels, P., Hendrix, A., De Boeck, A., V., M., Bracke, M., and De Wever, O. (2009) The extracellular matrix regulates cancer progression and therapy response:

Implications for prognosis and treatment. *Curr. Pharm. Des. 15*, 1373−1384.
(8) (2005) *Collagen: Primer in Structure, Processing, and Assembly* (Brickmann, J., Notbohm, H., and Müller, P. K., Eds.) Springer, New York.
(9) Chung, L., Dinakarpandian, D., Yoshida, N., Lauer-Fields, J. L., Fields, G. B., Visse, R., and Nagase, H. (2004) Collagenase unwinds triple-helical collagen prior to peptide bond hydrolysis. *EMBO J. 23*, 3020−3030.
(10) Rosenblum, G., Van den Steen, P. E., Cohen, S. R., Bitler, A., Opdenakker, G., Sagi, I., and Brand, D. D. (2010) Direct visualization of protease action on collagen triple helical structure. *PLoS One 5*, e11043.
(11) Orgel, J. P. R. O., Irving, T. C., Miller, A., and Wess, T. J. (2006) Microfibrillar structure of type I collagen in situ. *Proc. Natl. Acad. Sci. U.S.A. 103*, 9001−9005.
(12) Shoulders, M. D., and Raines, R. T. (2009) Collagen structure and stability. *Annu. Rev. Biochem. 78*, 929−958.
(13) Bella, J., Eaton, M., Brodsky, B., and Berman, H. M. (1994) Crystal and molecular structure of a collagen-like peptide at 1.9 Å resolution. *Science 266*, 75−81.
(14) Kramer, R. Z., Bella, J., Brodsky, B., and Berman, H. M. (2001) The crystal and molecular structure of a collagen-like peptide with a biologically relevant sequence. *J. Mol. Biol. 311*, 131−147.
(15) Kramer, R. Z., Vitagliano, L., Bella, J., Rita Berisio, R., Mazzarella, L., Brodsky, B., Zagari, A., and Berman, H. M. (1998) X-ray crystallographic determination of a collagen-like peptide with the repeating sequence (Pro-Pro-Gly). *J. Mol. Biol. 280*, 623−638.
(16) Berisio, R., Vitagliano, L., Mazzarella, L., and Zagari, A. (2001) Crystal structure of a collagen-like polypeptide with repeating sequence Pro-Hyp-Gly at 1.4 Å resolution: Implications for collagen hydration. *Biopolymers 56*, 8−13.
(17) Okuyama, K., Hongo, C., Fukushima, R., Wu, G., Narita, H., Noguchi, K., Tanaka, Y., and Nishino, N. (2004) Crystal structures of collagen model peptides with Pro-Hyp-Gly repeating sequence at 1.26 Å resolution: Implications for proline ring puckering. *Biopolymers 76*, 367−377.
(18) Kramer, R. Z., Bella, J., Mayville, P., Brodsky, B., and Berman, H. M. (1999) Sequence dependent conformational variations of collagen triple-helical structure. *Nat. Struct. Biol. 6*, 454−457.
(19) Saffarian, S., Collier, I. E., Marmer, B. L., Elson, E. L., and Goldberg, G. (2004) Interstitial collagenase is a brownian ratchet driven by proteolysis of collagen. *Science 306*, 108−111.
(20) Brodsky, B., and Persikov, A. V. (2005) Molecular structure of the collagen triple helix. *Adv. Protein Chem. 70*, 301−399.
(21) Brodsky, B., Thiagarajan, G., Madhan, B., and Kar, K. (2008) Triple-helical peptides: An approach to collagen conformation, stability, and self-association. *Biopolymers 89*, 345−353.
(22) Fields, G. B. (2010) Synthesis and biological applications of collagen-model triple-helical peptides. *Org. Biomol. Chem. 8*, 1237−1258.
(23) Lauer-Fields, J. L., Kele, P., Sui, G., Nagase, H., Leblanc, R. M., and Fields, G. B. (2003) Analysis of matrix metalloproteinase triple-helical peptidase activity with substrates incorporating fluorogenic L- or D-amino acids. *Anal. Biochem. 321*, 105−115.
(24) Lauer-Fields, J. L., Tuzinski, K. A., Shimokawa, K.-I., Nagase, H., and Fields, G. B. (2000) Hydrolysis of triple-helical collagen peptide models by matrix metalloproteinases. *J. Biol. Chem. 275*, 13282−13290.
(25) Lauer-Fields, J. L., Sritharan, T., Stack, M. S., Nagase, H., and Fields, G. B. (2003) Selective hydrolysis of triple-helical substrates by matrix metalloproteinase-2 and -9. *J. Biol. Chem. 278*, 18140−18145.
(26) Lauer-Fields, J. L., Broder, T., Sritharan, T., Chung, L., Nagase, H., and Fields, G. B. (2001) Kinetic analysis of matrix metalloproteinase activity using fluorogenic triple-helical substrates. *Biochemistry 40*, 5795−5803.
(27) Minond, D., Lauer-Fields, J. L., Nagase, H., and Fields, G. B. (2004) Matrix metalloproteinase triple-helical peptidase activities are differentially regulated by substrate stability. *Biochemistry 43*, 11474−11481.
(28) Ottl, J., Gabriel, D., Murphy, G., Knäuper, V., Tominaga, Y., Kröger, M., Tschesche, H., Bode, W., Moroder, L., and Nagase, H. (2000) Recognition and catabolism of synthetic heterotrimeric collagen peptides by matrix metalloproteinases. *Chem. Biol. 7*, 119−132.
(29) Lauer-Fields, J. L., Juska, D., and Fields, G. B. (2002) Matrix metalloproteinases and collagen catabolism. *Biopolymers 66*, 19−32.
(30) Brandstetter, H., Grams, F., Glitz, D., Lang, A., Huber, R., Bode, W., Krell, H.-W., and Engh, R. A. (2001) The 1.8-Å crystal structure of a matrix metalloproteinase 8-barbiturate inhibitor complex reveals a previously unobserved mechanism for collagenase substrate recognition. *J. Biol. Chem. 276*, 17405−17412.
(31) Chung, L., Shimokawa, K., Dinakarpandian, D., Grams, F., Fields, G. B., and Nagase, H. (2000) Identification of the (183)RWTNNFREY(191) region as a critical segment of matrix metalloproteinase 1 for the expression of collagenolytic activity. *J. Biol. Chem. 275*, 29610−29617.
(32) Bertini, I., Fragai, M., Luchinat, C., Melikian, M., Toccafondi, M., Lauer, J. L., and Fields, G. B. (2012) Structural basis for matrix metalloproteinase 1-catalyzed collagenolysis. *J. Am. Chem. Soc. 134*, 2100−2110.
(33) Manka, S. W., Carafoli, F., Visse, R., Bihan, D., Raynal, N., Farndale, R. W., Murphy, G., Enghild, J. J., Hohenester, E., and Nagase, H. (2012) Structural insights into triple-helical collagen cleavage by matrix metalloproteinase 1. *Proc. Natl. Acad. Sci. U.S.A. 109*, 12461−12466.
(34) McCawley, L. J., and Matrisian, L. M. (2001) Matrix metalloproteinases: They're not just for matrix anymore! *Curr. Opin. Cell Biol. 13*, 534−540.
(35) Overall, C. M., and Kleifeld, O. (2006) Validating matrix metalloproteinases as drug targets and anti-targets for cancer therapy. *Nat. Rev. Cancer 6*, 227−239.
(36) Suarez, E., Diaz, N., and Suarez, D. (2008) Entropic control of the relative stability of triple-helical collagen peptide models. *J. Phys. Chem. B 112*, 15248−15255.
(37) Rainey, J. K., and Goh, M. C. (2004) An interactive triple-helical collagen builder. *Bioinformatics 20*, 2458−2459.
(38) Rainey, J. K., and Goh, M. C. (2002) A statistically derived parameterization for the collagen triple-helix. *Protein Sci. 11*, 2748−2754.
(39) Case, D. A., Darden, T. A., Cheatham, T. E., III, Simmerling, C. L., Wang, J., Duke, R. E., Luo, R., Merz, K. M., Pearlman, D. A., Crowley, M., Walker, R. C., Zhang, W., Wang, B., Hayik, S., Roitberg, A., Seabra, G., Wong, K. F., Paesani, F., Wu, X., Brozell, S., Tsui, V., Gohlke, H., Yang, L., Tan, C., Mongan, J., Hornak, V., Cui, G., Beroza, P., Mathews, D. H., Schafmeister, C., Ross, W. S., and Kollman, P. A. (2006) *AMBER 9*, University of California, San Francisco.
(40) Duan, Y., Wu, C., Chowdhury, S., Lee, M. C., Xiong, G., Zhang, W., Yang, R., Cieplak, P., Luo, R., Lee, T., Caldwell, J., Wang, J., and Kollman, P. (2003) A point-charge force field for molecular mechanics simulations of proteins based on condensed-phase quantum mechanical calculations. *J. Comput. Chem. 24*, 1999−2012.
(41) Becke, A. D. (1988) Density-functional exchange-energy approximation with correct asymptotic behavior. *Phys. Rev. A 38*, 3098−3100.
(42) Kendall, R. A., Dunning, T. H., and Harrison, R. J. (1992) Electron affinities of the first-row atoms revisited. Systematic basis sets and wave functions. *J. Chem. Phys. 96*, 6796−6806.
(43) Cancès, M. T., Mennucci, B., and Tomasi, J. (1997) A new integral equation formalism for the polarizable continuum model: Theoretical background and applications to isotropic and anisotropic dielectrics. *J. Chem. Phys. 107*, 3032−3042.
(44) Bayly, C. I., Cieplak, P., Cornell, W. D., and Kollman, P. A. (1993) A well-behaved electrostatic potential based method using charge restraints for determining atom-centered charges: The RESP model. *J. Phys. Chem. 97*, 10269−10280.

(45) Wang, J., Wolf, R. M., Caldwell, J. W., Kollman, P. A., and Case, D. A. (2004) Development and testing of a general Amber force field. *J. Comput. Chem. 25*, 1157−1174.
(46) Wang, J., Cieplak, P., and Kollman, P. A. (2000) How well does a restrained electrostatic potential (RESP) model perform in calculating conformational energies of organic and biological molecules? *J. Comput. Chem. 21*, 1049−1074.
(47) Case, D. A., Darden, T. A., Cheatham, T. E., III, Simmerling, C. L., Wang, J., Duke, R. E., Luo, R., Crowley, M., Walker, R. C., Zhang, W., Merz, K. M., Wang, B., Hayik, S., Roitberg, A., Seabra, G., Kolossvary, K. F., Wong, K. F., Paesani, F., Vanicek, J., Wu, X., Brozell, S., Steinbrecher, T., Gohlke, H., Yang, L., Tan, C., Mongan, J., Hornak, V., Cui, G., Mathews, D. H., Seetin, M. G., Sagui, C., Babin, V., and Kollman, P. A. (2008) *AMBER 10*, University of California, San Francisco.
(48) Hawkins, G. D., Cramer, C. J., and Truhlar, D. G. (1996) Parametrized models of aqueous free energies of solvation based on pairwise descreening of solute atomic charges from a dielectric medium. *J. Phys. Chem. 100*, 19824−19839.
(49) Essmann, U., Perera, L., Berkowitz, M. L., Darden, T., Lee, H., and Pedersen, L. G. (1995) A smooth particle mesh Ewald method. *J. Chem. Phys. 103*, 8577−8593.
(50) Ryckaert, J.-P., Ciccotti, G., and Berendsen, H. J. C. (1977) Numerical integration of the cartesian equations of motion of a system with constraints: Molecular dynamics of n-alkanes. *J. Comput. Phys. 23*, 327−341.
(51) Phillips, J. C., Braun, R., Wang, W., Gumbart, J., Tajkhorshid, E., Villa, E., Chipot, C., Skeel, R. D., Kalé, L., and Schulten, K. (2005) Scalable molecular dynamics with NAMD. *J. Comput. Chem. 26*, 1781−1802.
(52) Diaz, N., and Suarez, D. (2008) Molecular dynamics simulations of the active matrix metalloproteinase-2: Positioning of the N-terminal fragment and binding of a small peptide substrate. *Proteins: Struct., Funct., Bioinf. 72*, 50−61.
(53) Babin, V., Roland, C., and Sagui, C. (2008) Adaptively biased molecular dynamics for free energy calculations. *J. Chem. Phys. 128*, 134101.
(54) Kumar, S., Rosenberg, J. M., Bouzida, D., Swendsen, R. H., and Kollman, P. A. (1995) Multidimensional free-energy calculations using the weighted histogram analysis method. *J. Comput. Chem. 16*, 1339−1350.
(55) Díaz, N., and Suárez, D. (2007) Molecular dynamics simulations of matrix metalloproteinase 2: The role of the structural metal ions. *Biochemistry 46*, 8943−8952.
(56) Gohlke, H., and Case, D. A. (2003) Converging free energy estimates: MM-PB(GB)SA studies on the protein−protein complex Ras −Raf. *J. Comput. Chem. 25*, 238−250.
(57) Hooft, R. W., Vriend, G., Sander, C., and Abola, E. E. (1996) Errors in protein structures. *Nature 381*, 272−272.
(58) Díaz, N., and Suárez, D. (2012) Alternative interdomain configurations of the full-length MMP-2 enzyme explored by molecular dynamics simulations. *J. Phys. Chem. B 116*, 2677−2686.
(59) Díaz, N., Suárez, D., and Valdés, H. (2008) From the X-ray compact structure to the elongated form of the full-length MMP-2 enzyme in solution: A molecular dynamics study. *J. Am. Chem. Soc. 130*, 14070−14071.
(60) Feig, M., Karanicolas, J., and Brooks, C. L. I. (2004) MMTSB tool set: Enhanced sampling and multiscale modeling methods for applications in structural biology. *J. Mol. Graphics Modell. 22*, 377−395.
(61) Kollman, P. A., Massova, I., Reyes, C., Kuhn, B., Huo, S., Chong, L., Lee, M., Lee, T., Duan, Y., Wang, W., Donini, O., Cieplak, P., Srinivasan, J., Case, D. A., and Cheatham, T. E. (2000) Calculating structures and free energies of complex molecules: Combining molecular mechanics and continuum models. *Acc. Chem. Res. 33*, 889−897.
(62) Sharp, K., and Honig, B. (1991) Electrostatic interactions in macromolecules: Theory and applications. *Annu. Rev. Biophys. Biophys. Chem. 19*, 301−332.
(63) Klein, T. E., and Huang, C. C. (1999) Computational investigations of structural changes resulting from point mutations in a collagen-like peptide. *Biopolymers 49*, 167−183.
(64) Li, M.-H., Fan, P., Brodsky, B., and Baum, J. (1994) Two-dimensional NMR assignments and conformation of (Pro-Hyp-Gly)lo and a designed collagen triple-helical peptide. *Biochemistry 32*, 7377−7387.
(65) Fiori, S., Saccà, B., and Moroder, L. (2002) Structural properties of a collagenous heterotrimer that mimics the collagenase cleavage site of collagen type I. *J. Mol. Biol. 319*, 1235−1242.
(66) Salsas-Escat, R., Nerenberg, P. S., and Stultz, C. M. (2010) Cleavage site specificity and conformational selection in type I collagen degradation. *Biochemistry 49*, 4147−4158.
(67) Xiao, J., Addabbo, R. M., Lauer, J. L., Fields, G. B., and Baum, J. (2010) Local conformation and dynamics of isoleucine in the collagenase cleavage site provide a recognition signal for matrix metalloproteinases. *J. Biol. Chem. 285*, 34181−34190.
(68) Nerenberg, P. S., and Stultz, C. M. (2008) Differential unfolding of α1 and α2 chains in type I collagen and collagenolysis. *J. Mol. Biol. 382*, 246−256.
(69) Bertini, I., Calderone, V., Fragai, M., Luchinat, C., Maletta, M., and Yeo, K. J. (2006) Snapshots of the reaction mechanism of matrix metalloproteinases. *Angew. Chem., Int. Ed. 45*, 7952−7955.
(70) Han, S., Makareeva, E., Kuznetsova, V., DeRidder, A. M., Sutter, M. B., Losert, W., Phillips, C. L., Visse, R., Nagase, H., and Leikin, S. (2010) Molecular mechanism of type I collagen homotrimer resistance to mammalian collagenases. *J. Biol. Chem. 285*, 22276−22281.
(71) Adhikari, A. S., Chai, J., and Dunn, A. R. (2011) Mechanical load induces a 100-fold increase in the rate of collagen proteolysis by MMP-1. *J. Am. Chem. Soc. 133*, 1686−1689.
(72) Müller, J. C., Ottl, J., and Moroder, L. (2000) Heterotrimeric collagen peptides as fluorogenic collagenase substrates: Synthesis, conformational properties, and enzymatic digestion. *Biochemistry 39*, 5111−5116.
(73) Gioia, M., Monaco, S., Fasciglione, G. F., Coletti, A., Modesti, A., Marini, S., and Coletta, M. (2007) Characterization of the mechanisms by which gelatinase A, neutrophil collagenase, and membrane-type metalloproteinase MMP-14 recognize collagen I and enzymatically process the two α-chains. *J. Mol. Biol. 368*, 1101−1113.
(74) Ottl, J., and Moroder, L. (1999) Disulfide-bridged heterotrimeric collagen peptides containing the collagenase cleavage site of collagen type I. Synthesis and conformational properties. *J. Am. Chem. Soc. 121*, 653−661.
(75) Díaz, N., and Suárez, D. (2008) Peptide hydrolysis catalyzed by matrix metalloproteinase 2: A computational study. *J. Phys. Chem. B 112*, 8412−8424.